Spatial beam self-cleaning in multimode fibres

K. Krupa[1,2]*, A. Tonello[1], B. M. Shalaby[1,3], M. Fabert[1], A. Barthélémy[1], G. Millot[2], S. Wabnitz[4,5] and V. Couderc[1]

Multimode optical fibres are enjoying renewed attention, boosted by the urgent need to overcome the current capacity crunch of single-mode fibre (SMF) systems and by recent advances in multimode complex nonlinear optics[1–13]. In this work, we demonstrate that standard multimode fibres (MMFs) can be used as ultrafast all-optical tools for the transverse beam manipulation of high-power laser pulses. Our experimental data show that the Kerr effect in a graded-index (GRIN) MMF is the driving mechanism that overcomes speckle distortions, and leads to a counterintuitive effect that results in a spatially clean output beam robust against fibre bending. Our observations demonstrate that nonlinear beam reshaping into the fundamental mode of a MMF can be achieved even in the absence of a dissipative process such as stimulated scattering (Raman or Brillouin)[14,15].

Beam propagation in MMFs is subject to a complex interplay of spatiotemporal processes. However, only a few studies have addressed nonlinear pulse propagation in MMFs, a field largely untapped for the past 30 years. Very recently, there has been a resurgence of interest in MMFs for both fundamental and applied research. MMFs could provide a solution to meet the increasing demands of new breakthrough technologies for light control and manipulation in communications, high-power fibre lasers and metrology[1,2,16]. In fundamental physics, MMFs may provide a natural tool to investigate spatiotemporal soliton dynamics[5,6] and to unveil new, exciting nonlinear phenomena[3,4,9,13].

It is well known that light experiences an inherent randomization when propagated along MMFs, whereby the input laser beams of high spatial quality fade into irregular granularities called speckles. Fibre stress or bending, as well as technological irregularities of the fibre, couple different guided modes and introduce supplementary randomization of the transmission features. For this reason, MMFs are not ideally suited for beam delivery and SMFs have been used since the early days of optical communications. Recent works demonstrated that specific signal-processing algorithms could be used to predict or manage the beam shape at the output of a MMF by controlling its input field[17–19]. In particular, the application of multiple-input, multiple-output (MIMO) digital signal-processing techniques enables the use of spatial-division multiplexing based on MMFs[2]. For high-power beam delivery applications, the spontaneous recovery of spatial beam quality in MMFs has so far been achieved experimentally exclusively through nonlinear dissipative processes such as stimulated Raman scattering (SRS)[14] or stimulated Brillouin scattering[20]. However, these techniques do not lead to any self-cleaning of the input laser beam. It is now known that for powers above a critical level (a few megawatts), self-phase modulation (SPM) may overcome diffraction for any size of the beam, which may in turn collapse into a filament. Lushnikov and Vladimirova[21] proposed the use of this effect to combine multiple laser beams into a single one. Recent experiments reported supercontinuum generation of femtosecond light pulses in the anomalous dispersion regime of GRIN MMFs: the close resemblance to self-focusing and multiple filamentation suggested the potential role of GRIN MMFs in achieving beam clean-up through the control of the input launching conditions[3,4].

In this Letter, we demonstrate experimentally that a single strong laser beam can display enhanced brightness when propagating through MMFs. We show a new regime of remarkably stable self-induced bell-shaped beam propagation in MMFs based on the nonlinear non-reciprocity of mode coupling that occurs in the normal dispersion regime.

In our experiments, we launched intense laser pulses with a temporal duration of 900 ps and a wavelength of 1,064 nm into a standard 12-m-long GRIN MMF. Using a wide-input Gaussian beam of about 40 μm in diameter, we simultaneously excited about 200 guided modes on both polarization components. Figure 1a–d shows the transverse spatial beam intensity at 1,064 nm as a function of the output peak power (P_{PP}); the corresponding beam transverse profiles are displayed in Fig. 1e–h, respectively. At relatively low power ($P_{PP} = 3.7$ W), the smooth-input Gaussian beam evolved into an irregular transverse profile with several randomly distributed speckles at the output (Fig. 1a,e). As we increased the input power, the beam profile coalesced from a highly irregular to a well-defined bell-shaped structure in the core centre, surrounded by a low-power speckled pedestal, as shown in Fig. 1d,h (Supplementary Movie 1). We did not observe any significant change in the input/output power-transmission ratio between the low- and the high-intensity excitation regimes. Importantly, this rules out the possibility of a beam self-cleaning effect because of a higher level of nonlinear loss for the high-order modes (HOMs) relative to the fundamental mode. We performed a simultaneous spatial and spectral analysis with a dispersive spectroscope and carried out Young's double-slit experiment to verify that the redistribution of power towards a central quasi-Gaussian profile results neither from spectral broadening and loss of temporal coherence, nor from loss of spatial coherence. As presented in Fig. 2a,b, spatial beam self-cleaning occurs with the frequency spectrum virtually unchanged. Further, we obtained interference fringes with a similar contrast of 70% when the two interfering parts of either the initial speckled beams or of the self-cleaned beams were spaced by a distance nearly equal to the beam diameter taken at the full-width at half-maximum intensity (FWHMI) (Fig. 2c,d and Supplementary Information). The observed behaviour resembles the effect of multimode wave condensation, which was theoretically predicted in ref. 22 in the continuous-wave limit, whereby an initial random distribution of guided modes exhibits an irreversible evolution towards an equilibrium state. In this state, the fundamental mode grows to a dominant level of occupation while remaining immersed in a sea of small-scale fluctuations. In Fig. 3a, we illustrate the

---

[1]Université de Limoges, XLIM, UMR CNRS 7252, 123 Avenue A. Thomas, 87060 Limoges, France. [2]Université de Bourgogne Franche-Comté, ICB, UMR CNRS 6303, 9 Avenue A. Savary, 21078 Dijon, France. [3]Physics Department, Faculty of Science, Tanta University, 31527 Tanta, Egypt. [4]Dipartimento di Ingegneria dell'Informazione, Università di Brescia, and INO-CNR, via Branze 38, 25123 Brescia, Italy. [5]Novosibirsk State University, 1 Pirogova str., Novosibirsk 630090, Russia. *e-mail: katarzyna.krupa@u-bourgogne.fr
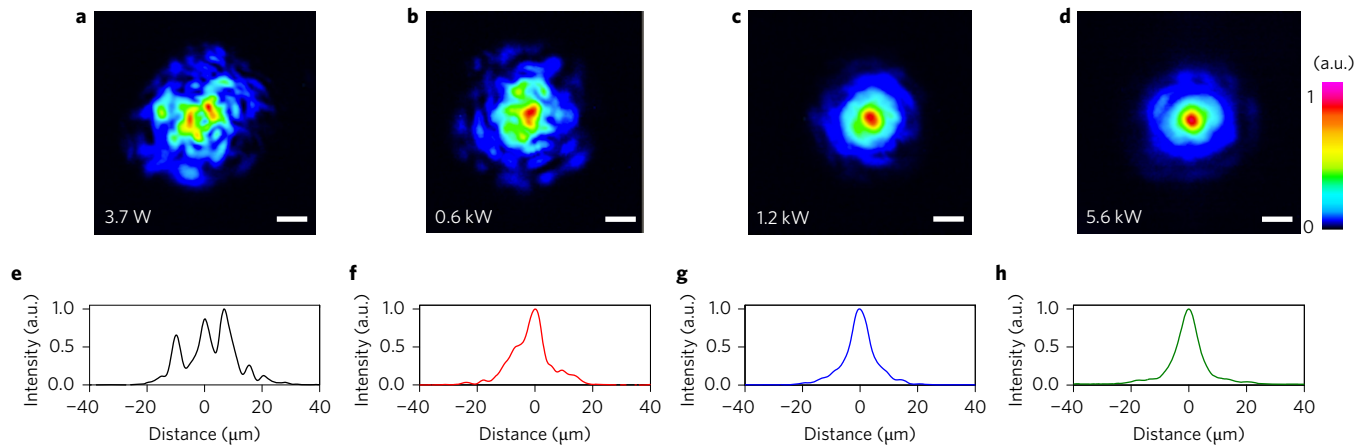
Figure 1 | Experimental nonlinear dynamics of beam self-cleaning in a GRIN MMF. a–d, Near-field images of the MMF output recorded at 1,064 nm (intensities are referred to the local maximum and are shown on a linear scale) show spatial beam self-cleaning, namely the formation of a well-defined bell-shaped transverse beam distribution when the output peak power P_{PP} is increasing. Scale bars, 10 µm. **e–h**, Corresponding beam profiles versus x ($y = 0$ section). Fibre length, 12 m.
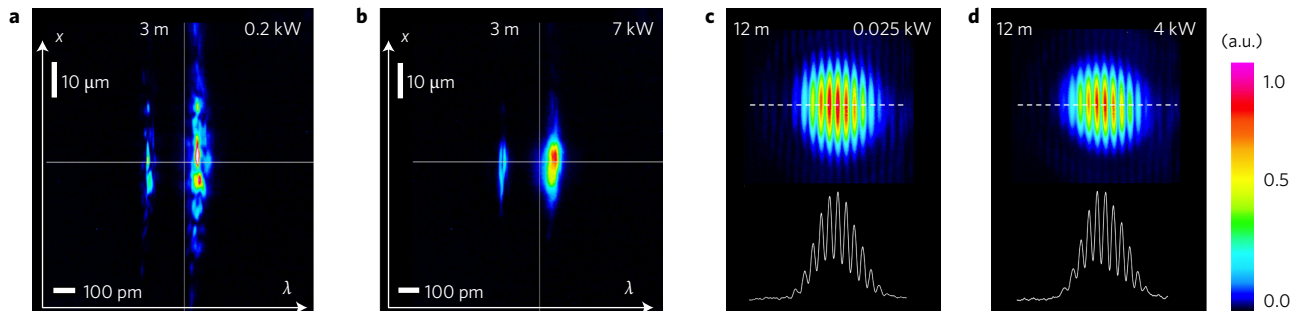

Figure 2 | Experimental analysis of temporal and spatial coherence of beam self-cleaning in a GRIN MMF. a,b, Spatiospectral (x–λ) profile of the output wave in a linear propagation regime at the output peak power $P_{PP} = 0.2$ kW (**a**) and in the beam self-cleaning regime at $P_{PP} = 7$ kW (**b**). Fibre length, 3 m. The output spectrum is essentially characterized by a nearly single longitudinal mode of the microchip laser with a weak second longitudinal mode. **c,d**, Examples of near-field interference patterns obtained in Young's double-slit experiment; the corresponding x-axis cross section is obtained either in the linear propagation regime at the output peak power $P_{PP} = 0.025$ kW (**c**) or in the beam self-cleaning regime at $P_{PP} = 4$ kW (**d**). Fibre length, 12 m.

dependence of the output near-field beam FWHMI diameters on the output power, for an input beam condition that leads to a largely extended speckle pattern at low powers (filled red circles in Fig. 3a); a similar behaviour was observed in the far-field region. To study the dependence of beam self-cleaning on the input launching conditions, we measured the output beam diameter for each considered power value based on a large, statistically significant number (1,000) of different input beams (which lead to different energy distributions among the guided modes). From Fig. 3b, one can see that at high powers there is a significant reduction in the average beam diameter, as well as a dramatic reduction in the corresponding standard deviation (Supplementary Information).

Additionally, we carried out numerical studies (Supplementary Information), which indicated that the bell-shaped self-cleaned beam is essentially composed of the fundamental mode instead of a coherent summation of a few low-order modes. Indeed, simulations show that at large input beam powers the relative contribution of the fundamental mode to the output beam power is significantly enhanced, whereas the power contribution from other modes progressively decreases. This prediction is confirmed by our experimentally measured self-cleaned beam diameter of 7.8 µm FWHMI (Fig. 3a), which closely matches the theoretical value of the beam diameter for the fundamental mode of the considered GRIN fibre (7.45 µm FWHMI)[23]. The coalescence into the fundamental mode first appeared at a power level of $P_{PP} = 0.6$ kW (Fig. 3a), which is

well below the threshold for SRS (in our case, the initial formation of the first Raman Stokes sideband took place at $P_{PP} = 5.6$ kW), as well as the catastrophic self-focusing threshold (in the megawatt region)[21]. In the spectral domain, the beam self-cleaning process was accompanied by a weak symmetrical spectral broadening of the pedestal, localized at more than 15 dBs below the laser beam (Supplementary Fig. 8a). Additionally, we observed that beam self-cleaning was very robust on further manual squeezing and bending of the fibre (Supplementary Movie 2). This behaviour drastically differs from the common situation found in the linear regime, in which the output beam is characterized by speckles that result from the linear interference of many excited modes (Supplementary Movie 2). It is important to note that linear coupling among guided modes was neglected in ref. 22, whereas it is definitely present in our experiments. In this sense, the beam self-cleaning effect is observed in situations that are considerably more complex than the framework under which the theory of classical wave condensation was originally formulated.

The observed self-induced spatial-cleaning effect significantly enhances the output beam spatial quality, as indicated by the simultaneous concentration of energy in the near field and in the far field. To emphasize this effect, we measured the fraction of power at 1,064 nm carried by the central part of the beam (selected with a diaphragm opened at a diameter of 12 µm) to increase input powers, and compared it with the total output power at 1,064 nm.
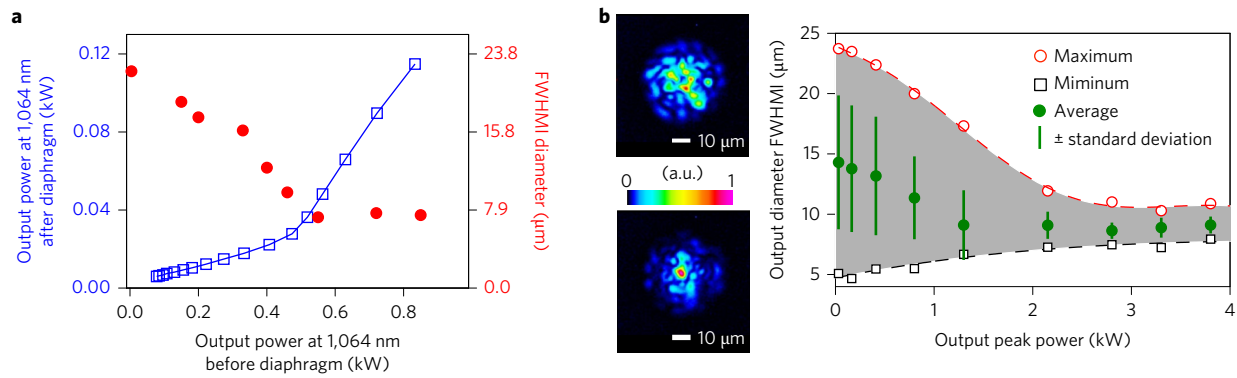
Figure 3 | Brightness enhancement and statistical analysis of beam self-cleaning in a GRIN MMF. a, Output power at 1,064 nm measured in the central part of the fibre as a function of the total output power (blue open squares), and corresponding FWHMI diameters of the near-field beam (at 1,064 nm) (red filled circles). Brightness enhancement is demonstrated by the net increase of the slope of the blue curve. **b,** Average values of the FWHMI diameter as a function of the output power, calculated from 1,000 different input conditions, with the corresponding standard deviations, as well as maximum and minimum diameter values. The red and black dotted curves are fits to guide the eye. Insets: examples of near-field images illustrating two 'extreme' spatial beam distributions with maximum (top inset; corresponding to red circles) and minimum (bottom inset; corresponding to black squares) diameters recorded at a low peak power of $P_{PP} = 0.1$ kW. Fibre length, 12 m.
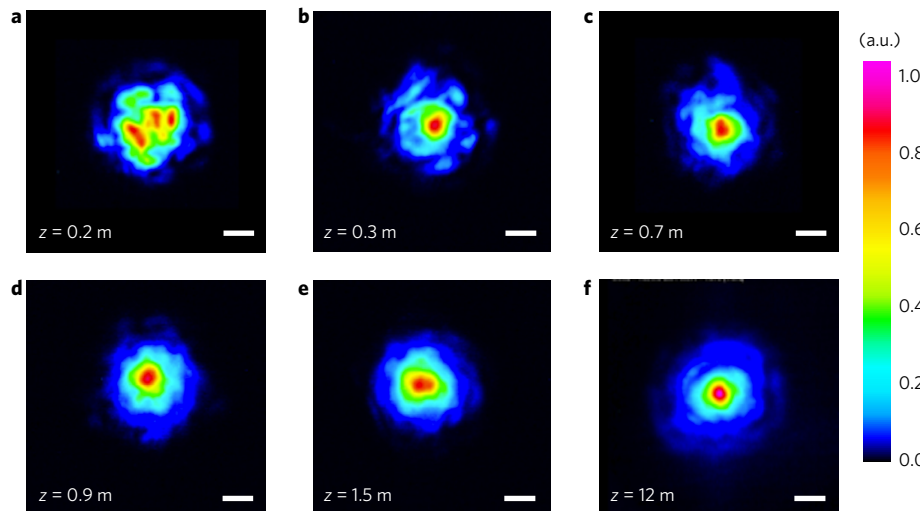

Figure 4 | Experimental cut-back analysis of beam propagation in a GRIN MMF. a–f, Near-field images recorded at 1,064 nm (normalized intensity on a linear scale) show the development of beam self-cleaning along the propagation distance z. Output peak power at z = 12 m is $P_{PP} = 44$ kW (that is, high power). Scale bars, 10 μm.

The data points given by the blue open squares in Fig. 3a show that the power in the centre of the beam increases nearly linearly with the fibre output power up to the power threshold $P_{Th} \approx 0.5$ kW, where an abrupt increment in slope by a factor 5.3 confirms an enhancement of the beam brightness. The linear behaviour beyond P_{Th} indicates the establishment of a new equilibrium in the energy distribution between HOMs and the fundamental mode. This suggests that the process has a non-catastrophic nature, similarly to multimode-wave condensation[22]. By contrast, a nonlinear beam-narrowing behaviour with increasing propagation distance is typically expected for catastrophic effects such as self-focusing.

For further insights into the nonlinear mechanism at the basis of beam self-cleaning, we studied the evolution of the spatial beam profile along the MMF by gradually backward cutting the fibre. The experimental results obtained at $P_{PP} = 44$ kW are shown in Fig. 4. Despite the relatively high power used in these experiments, the input Gaussian beam still splits into several guided modes along the first few hundreds of millimetres to produce spatial speckles (Fig. 4a). The observed scrambling of the initial phase front proves that, immediately after coupling light into the fibre, transverse beam evolution is predominantly affected by mode beating owing to their different wavenumbers. Progressing further along the fibre, our cut-back analysis reveals that a strong modification of the modal intensity distribution takes places: the brightness of the output beam increases despite the remaining weak random-speckle background.

Spatial beam Kerr self-cleaning may be explained in terms of the nonlinear non-reciprocity of the mode-coupling process[24]. In fibres with a parabolic index profile, the propagation constants of the modes take equally spaced values so that coherent mode beating induces a periodic local intensity oscillation along the fibre, which the Kerr effect translates into a periodic longitudinal modulation of the refractive index[4,10,12]. With a simpler two-mode excitation, this type of self-induced or dynamic long-period Bragg grating was exploited previously to demonstrate light-controlled mode conversion in a GRIN MMF[25]. More generally, four-wave mixing
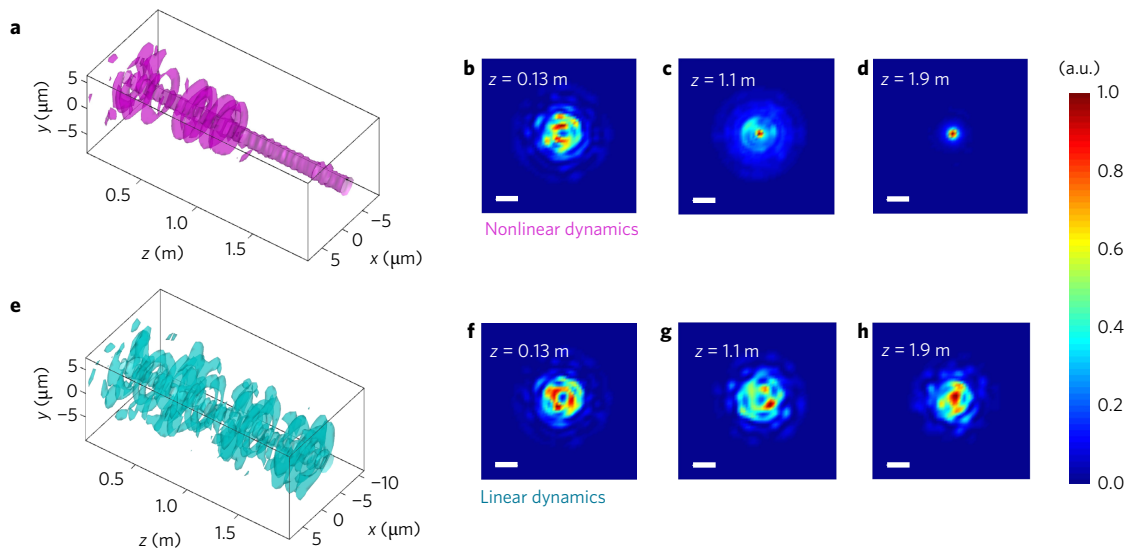
Figure 5 | Numerical results of beam propagation in a GRIN MMF. a–h, Spatial reshaping along the propagation distance z shows the emergence of beam self-cleaning in the nonlinear regime (**a**), whereas no self-cleaning occurs in the linear regime (**e**). Isosurfaces represent points at 70% of the local maximum intensity value. Two-dimensional output distributions in the nonlinear (**b–d**) and linear (**f–h**) regimes. The input peak power is 63 kW (that is, intensity I = 5 GW cm^{-2}). Spatial frames are obtained by averaging the time-integrated intensity along z over three consecutive samples (spaced by 5 mm). Scale bars, 10 μm.

(FWM) interactions that involve pairs of beating modes at the same wavelength introduce Bragg-type quasi-phase-matching conditions for a variety of mode-coupling processes. As a result, energy exchanges occur between the forward-propagating fundamental mode and the HOMs. We derived (Supplementary Information) a simplified two-mode mean-field model that makes it possible to describe analytically the dynamics of the interaction between the fundamental mode and the HOMs—in terms of an effective coupling term—driven by the collective presence of all-fibre modes through FWM. Mean-field theory (MFT) allows us to study the behaviour of large complex models in terms of a much simpler model; with this approach, the interaction of a large number of modes with the fundamental mode is approximated as a single averaged effect. A key outcome of the MFT that explains the observed Kerr self-cleaning effect is the nonlinear non-reciprocal behaviour of the equivalent nonlinear two-mode coupler model. Nonlinear non-reciprocity arises precisely because of the presence of SPM, which is highly different for the fundamental and for the HOMs owing to the difference between their overlap integrals. Specifically, nonlinear non-reciprocal coupling behaviour manifests as follows. For a specific and sufficiently large input total power, if the mode power distribution is initially in favour of the HOMs (Supplementary Fig. 4d), then one observes periodic power exchange between the fundamental and the HOMs. However, if the initial power distribution is in favour of the fundamental mode (Supplementary Fig. 4c), the beam power remains in the fundamental mode. This non-reciprocity is nonlinear in that it only manifests above a given threshold power, a fact that is in qualitative agreement with our experiments. One can further speculate that, when extended to describe the collective interactions in the original complex multimode system, the nonlinear non-reciprocity of the MFT model smoothens the dependence on the initial conditions and leads to irreversibility of the energy flow into the fundamental mode. In Bose–Einstein condensates[26], the macroscopic quantum self-trapping of an initial population imbalance occurs because of interatomic interaction in the Bose gas. The self-cleaning process may thus be seen as an analogous phenomenon for the ensemble of photons in a MMF.

Our experimental observations are qualitatively well reproduced by numerical simulations performed by solving a generalized version of the nonlinear Schrödinger equation (GNLSE3D) that comprises two transverse spatial coordinates, x,y (to account for the spatial beam distribution), the temporal variable t and the propagation coordinate z (refs 6,23,27–29). Numerical simulations of spatial and spectral beam evolution along the fibre are displayed in Fig. 5. Figure 5a–d show that the initially highly multimodal distribution of the laser beam inside the MMF is gradually 'attracted' towards a bell-shaped transverse profile, in agreement with our experiments. The power of the fundamental mode increases by a factor of ~2.3 after 1 m of propagation distance (Supplementary Information). To show that beam self-cleaning only results from Kerr dynamics and that SRS does not drive it, we limited the peak power to below the Raman threshold ($P_{PP} < 5.6$ kW) for most of the experiments presented here. Therefore, we did not include SRS in our simulations. For ease of comparison, in Fig. 5e–h we report the numerical simulations with a relatively low intensity, that is, in the linear regime (Supplementary Movie 3).

In conclusion, we demonstrated experimentally light self-cleaning, which enables a robust effective propagation of spatially bell-shaped beams despite the high number of permitted guided modes. Our observations may pave the way to develop novel photonic devices for a wealth of applications, based on combining an effective spatial single-mode environment with large fibre-core diameters. From a fundamental perspective, beam self-cleaning is similar to the condensation of multimode waves[22,30], which is formally equivalent to the Bose–Einstein condensation of gas particles. Complex multimode dynamics may shed new light on exciting physical phenomena such as spatiotemporal solitons[6–8] and spatiotemporal rogue waves and turbulence[31], as well as extend the synchronization of coupled nonlinear oscillators (described by the Kuramoto model[32], for example) to spatially extended natural systems. The presented results may also stimulate further theoretical analysis of the complex interactions at play in nonlinear multimode systems.

Methods

Methods and any associated references are available in the online version of the paper.

References

1. Richardson, D. J., Nilsson, J. & Clarkson, W. A. High power fiber lasers: current status and future perspectives. *J. Opt. Soc. Am. B* **27,** B63–B92 (2010).
2. Richardson, D. J., Fini, J. M. & Nelson, L. E. Space division multiplexing in optical fibers. *Nat. Photon.* **7,** 354–362 (2013).
3. Wright, L. G., Christodoulides, D. N. & Wise, F. W. Controllable spatiotemporal nonlinear effects in multimode fibres. *Nat. Photon.* **9,** 306–310 (2015).
4. Wright, L. G., Wabnitz, S., Chistodoulides, D. N. & Wise, F. W. Ultrabroadband dispersive radiation by spatiotemporal oscillation of multimode waves. *Phys. Rev. Lett.* **115,** 223902 (2015).
5. Renninger, W. H. & Wise, F. W. Optical solitons in graded-index multimode fibres. *Nat. Commun.* **4,** 1719 (2013).
6. Yu, S.-S., Chien, Ch.-H., Lai, Y. & Wang, J. Spatio-temporal solitary pulses in graded-index materials with Kerr nonlinearity. *Opt. Commun.* **119,** 167–170 (1995).
7. Gurgov, H. C. & Cohen, O. Spatiotemporal pulse-train solitons. *Opt. Express* **17,** 7052–7058 (2009).
8. Burgess, I. B., Peccianti, M., Assanto, G. & Morandotti, R. Accessible light bullets via synergetic nonlinearities. *Phys. Rev. Lett.* **102,** 203903 (2009).
9. Picozzi, A., Millot, G. & Wabnitz, S. Nonlinear virtues of multimode fibre. *Nat. Photon.* **9,** 289–291 (2015).
10. Longhi, S. Modulational instability and space–time dynamics in nonlinear parabolic-index optical fibers. *Opt. Lett.* **28,** 2363–2365 (2003).
11. Buch, S. & Agrawal, G. P. Soliton stability and trapping in multimode fibers. *Opt. Lett.* **40,** 225–228 (2015).
12. Krupa, K. *et al.* Observation of geometric parametric instability induced by the periodic spatial self-imaging of multimode waves. *Phys. Rev. Lett.* **116,** 183901 (2016).
13. Wright, L. G. *et al.* Self-organized instability in graded-index multimode fibres. *Nat. Photon.* **10,** 771–776 (2016).
14. Chiang, K. S. Stimulated Raman scattering in a multimode optical fiber: self-focusing or mode competition? *Opt. Commun.* **95,** 235–238 (1993).
15. Terry, N. B., Alley, T. G. & Russell, T. H. An explanation of SRS beam cleanup in graded-index fibers and the absence of SRS beam cleanup in step-index fibers. *Opt. Express* **15,** 17509–17519 (2007).
16. Barmes, I., Witte, S. & Eikema, K. S. E. Spatial and spectral coherent control with frequency combs. *Nat. Photon.* **7,** 38–42 (2013).
17. Mahalati, R. N., Askarov, D., Wilde, J. P. & Kahn, J. M. Adaptive control of input field to achieve desired output intensity profile in multimode fiber with random mode coupling. *Opt. Express* **20,** 14321–14337 (2012).
18. Papadopoulos, I. N., Farahi, S., Moser, Ch. & Psaltis, D. Focusing and scanning light through a multimode optical fiber using digital phase conjugation. *Opt. Express* **20,** 10583–10590 (2012).
19. Plöschner, M., Tyc, T. & Čižmár, T. Seeing through chaos in multimode fibres. *Nat. Photon.* **9,** 529–535 (2015).
20. Lombard, L., Brignon, A., Huignard, J.-P. & Lallier, E. Beam cleanup in a self-aligned gradient-index Brillouin cavity for high-power multimode fiber amplifiers. *Opt. Lett.* **31,** 158–160 (2006).
21. Lushnikov, P. M. & Vladimirova, N. Nonlinear combining of laser beams. *Opt. Lett.* **39,** 3429–3432 (2014).
22. Ascheri, P., Garnier, G., Michel, C., Doya, V. & Picozzi, A. Condensation and thermalization of classical optical waves in a waveguide. *Phys. Rev. A* **83,** 033838 (2011).
23. Mafi, A. Pulse propagation in a short nonlinear graded-index multimode optical fiber. *J. Light. Technol.* **30,** 2803–2811 (2012).
24. Trillo, S. & Wabnitz, S. Nonlinear nonreciprocity in a coherent mismatched directional coupler. *Appl. Phys. Lett.* **49,** 752–754 (1986).
25. Hellwig, T., Schnack, M., Walbaum, T., Dobner, S. & Fallnich, C. Experimental realization of femtosecond transverse mode conversion using optically induced transient long-period grating. *Opt. Express* **22,** 24951–24958 (2014).
26. Anglin, J. R. & Vardi, A. Dynamics of a two-mode Bose-Einstein condensate beyond mean-field theory. *Phys. Rev. A* **64,** 013605 (2001).
27. Poletti, F. & Horak, P. Dynamics of femtosecond supercontinuum generation in multimode fibers. *Opt. Express* **17,** 6134–6147 (2009).
28. Marcuse, D. *Theory of Dielectric Optical Waveguides* (Academic, 1974).
29. Modotto, D. *et al.* Ge-doped microstructured multicore fiber for customizable supercontinuum generation. *IEEE Photon. J.* **3,** 1149–1156 (2011).
30. Sun, C. *et al.* Observation of the kinetic condensation of classical waves. *Nat. Phys.* **8,** 470–474 (2012).
31. Picozzi, A. *et al.* Optical wave turbulence: towards a unified nonequilibrium thermodynamic formulation of statistical nonlinear optics. *Phys. Rep.* **542,** 1–132 (2014).
32. Acebron, J. A., Bonilla, L. L., Pérez Vicente, C. J., Ritort, F. & Spigler, R. The Kuramoto model: a simple paradigm for synchronization phenomena. *Rev. Mod. Phys.* **77,** 137–185 (2005).

Author contributions

K.K. and V.C. carried out the experiments. A.T. and S.W. performed the numerical simulations and theoretical analysis. All the authors analysed and interpreted the obtained results, and participated equally in the discussions and in the writing of the manuscript.

Additional information

Supplementary information is available in the online version of the paper. Reprints and permissions information is available online at www.nature.com/reprints. Publisher's note: Springer Nature remains neutral with regard to jurisdictional claims in published maps and institutional affiliations. Correspondence and requests for materials should be addressed to K.K.

Competing financial interests

The authors declare no competing financial interests.

Methods

Experimental set-up. We used a standard, commercially available GRIN MMF of 12 m length, 52.1 μm core diameter and 0.205 NA. The fibre was intentionally wound and bent in a fibre bundle to excite a large number of guided modes (~200), and also to investigate the influence of mechanical deformations (strong linear coupling) on beam self-cleaning. In GRIN MMFs, the maximum temporal broadening caused by modal dispersion is expected to be in the range of 12 ps for 12 m of fibre. Therefore, modal dispersion can be neglected in our experiments. The laser source was an amplified neodymium–yttrium-aluminium-garnet microchip laser that delivered 900 ps pulses at 1,064 nm and a 30 kHz repetition rate. The polarized Gaussian laser pulses were launched into the fibre by using a lens with a focal length of 50 mm and a three-axis translation stage. At the input face of the fibre, the beam had a FWHMI diameter of 40 μm, which was close to the value of the fibre-core diameter. The translating stage also allowed control over the initial spatial coupling condition by adjusting the relative position between the fibre and the launched beam. We used an optical spectrum analyser that covered the spectral range from 350 nm to 1,750 nm. The near-field beam profile (at the output face of the fibre) was imaged on a charge-coupled device camera through an 8 mm microlens with a magnification of $G = 41$. A 10-nm-wide bandpass interference optical filter at 1,064 nm was introduced to analyse the spatial dynamics at the laser wavelength. In our experiment, owing to the long pulse duration of the laser source and the low modal dispersion ensured by the parabolic profile of the fibre refractive index, a large number of initially excited modes could keep their temporal superposition, and hence a strong nonlinear coupling, for several tens of metres. To measure the fraction of power at 1,064 nm carried by the central part of the beam (Fig. 3a), we filtered the 82 times magnified output near field with a diaphragm of ~1 mm radius, which corresponds to a sensitive disc area of 12 μm diameter on the fibre-exit face.

Numerical simulations. We numerically solved the GNLSE3D, which is an envelope equation that stems from Maxwell's equations under the paraxial and unidirectional propagation approximations, with a nonlinear polarization limited to frequency components around the carrier wavelength of the laser beam. We used an integration step of 0.05 mm and a transverse 128×128 grid for a spatial window of 150×150 μm. We considered a standard GRIN MMF with a core radius $\rho = 26$ μm and a maximum value for the core refractive index $n_{co} = 1.47$, and for the cladding index $n_{cl} = 1.457$. We took a truncated parabolic profile of the refractive index in the transverse domain: $n(x,y)^2 = n_{co}^2(1 - 2\Delta r^2/\rho^2)$ for $r < \rho$ and $n(x,y) = n_{cl}$ otherwise, where $r^2 = x^2 + y^2$ and $\Delta = 8.8 \times 10^{-3}$. For simplicity, we retained the frequency dependence of the silica refractive index only through the group velocity-dispersion term at 1,064 nm, $\kappa'' = 16.55 \times 10^{-27}$ s^2 m^{-1} and limited our numerical analysis to the scalar case, that is, we neglected the polarization state of light. We considered a non-dispersive Kerr nonlinear index, $n_2 = 3.2 \times 10^{-20}$ m^2 W^{-1} and a Raman fraction $f_R = 0.18$ (in the absence of Raman, the Kerr nonlinear index was still reduced by a factor $1 - f_R$). We used an input beam diameter of 40 μm. To reduce the computational time, we rescaled the problem by using an input intensity $I = 5$ GW cm^{-2} (that is, a peak power of 63 kW), higher than that used in our experiments, to reduce the propagation length to a maximum value of $L = 2$ m, and we used a pulse duration of 7.5 ps. To mimic the speckled near-field image observed at low peak powers, we used two different approaches that gave similar numerical results. The results presented in the main text of the Letter were obtained with the first technique, in which we blurred an input flat spatial phase front with a random uniformly distributed two-dimensional function and solved the GNLSE3D equation with constant coefficients, as would happen in an ideal fibre in the absence of linear coupling among the guided modes. In this case, the multiplicative input phase noise is intended to imitate the phase shifts in the first steps of propagation in the fibre. In the second approach, we applied a coarse-step distributed coupling method that started from a coherent input condition represented by a flat phase and Gaussian intensity distribution, and perturbed the propagation by randomly changing selected key parameters, such as the fibre core diameter or the relative refractive index difference, as well as by introducing random artificial tilts to the beam in the fibre. We introduced these numerical perturbations every 1 mm, which is much longer than our basic integration step. The corresponding numerical results are given in the Supplementary Information.

Data availability. The data that support the plots within this paper and other findings of this study are available from the corresponding author on reasonable request.